Regular Article

Vlasov description of the beam response to noise in the presence of wakefields in high-energy synchrotrons: beam transfer function, diffusion, and loss of Landau damping

Sondre Vik Furuseth[1,2,a] , **Xavier Buffat**[1]

[1] The European Organization for Nuclear Research (CERN), 1211 Geneva 23, Switzerland
[2] École polytechnique fédérale de Lausanne (EPFL), 1015 Lausanne, Switzerland

Abstract Noise can have severe impacts on particle beams in high-energy synchrotrons. In particular, it has recently been discovered that noise combined with wakefields can cause a diffusion that leads to a loss of Landau damping after a latency. Such instabilities have been observed in the Large Hadron Collider. This paper, therefore, studies the beam response to noise in the presence of wakefields, within the framework of the Vlasov equation. First, a wakefield beam eigenmode transfer function (MTF) is derived, quantifying the amplitude of a wakefield eigenmode when excited by noise. Then, the MTFs of all the wakefield eigenmodes are combined to derive the beam transfer function (BTF) including the impact of wakefields. It is found to agree excellently with multi-particle tracking simulations. Finally, the MTFs are also used to derive the single-particle diffusion driven by the wakefield eigenmodes. This new Vlasov-based theory for the diffusion driven by noise-excited wakefields is found to be superior to an existing theory by comparing to multi-particle tracking simulations. Through sophisticated simulations that self-consistently model the evolution of the distribution and the stability diagram, the diffusion is found to lead to a loss of Landau damping after a latency. The most important technique to extend the latency and thereby mitigate these instabilities is to operate the synchrotron with a stability margin in detuning strength relative to the amount of detuning required to barely stabilize the beam with its initial distribution.

1 Introduction

The impact of various noise sources on the beams in high-energy synchrotrons has been studied extensively in the past. Typically, the focus is on the consequent emittance growth and reduction of luminosity in colliders, or alternatively on how this emittance growth can be suppressed with feedback systems. Recently, it has also been found that the interplay between noise and wakefields can cause instabilities that occur after a latency. Such instabilities have been observed in the Large Hadron Collider (LHC), both in operation and in dedicated experiments [1,2], and the mechanism behind has been explained semi-analytically [3,4]. This mechanism is a major concern for the high-luminosity LHC (HL-LHC), which will have beams of higher brightness and also new components such as crab cavities that will introduce a new type of noise. Therefore, we need a better understanding of how the noise excites the beam, including the interplay with other mechanisms. Here, the focus is on the interplay with wakefields.

In this paper, we study the evolution of beam distribution perturbations within the framework of the linear Vlasov equation, as in Ref. [5]. In the absence of wakefields, we use this framework to re-derive the beam transfer function (BTF) [6,7] including linear chromaticity [8]. The BTF is the amplitude of the transverse betatron oscillation of the beam at a certain frequency, relative to the excitation amplitude at that frequency. When we include the wakefields, the distribution perturbations become wakefield-driven beam eigenmodes. We derive what we call the wakefield beam eigenmode transfer function (MTF), which is the BTF equivalent for each eigenmode separately, also taking into consideration the dependence of the modes on the longitudinal coordinates. Based on the MTFs of all the eigenmodes, we arrive at an expression for the BTF including wakefields. This new theory explains observations made in experiments in the past, highlighting the impact of the wakefields on the BTF. With this understanding of the impact of wakefields, the multi-purpose diagnostic tool that is the BTF can be applied more precisely.

By extending the Vlasov equation to second order, we effectively arrive at a Fokker–Planck equation modeling a diffusion driven by noise and wakefields. It was found in Ref. [3] that the diffusion coefficient related to an almost unstable mode is peaked and narrow in tune space. When there is *e.g.* a vertical detuning proportional to the vertical action, this diffusion causes a local flattening of the distribution as the particles are evenly distributed over the vertical actions corresponding to the tunes of largest diffusion coefficient. The distribution modification corresponds to a modification of the stability diagram [6], eventually leading to a loss of Landau damping. The MTFs based on the linear Vlasov equation is in this paper used to derive a new expression for this diffusion,

[a] e-mail: s.v.furuseth@gmail.com (corresponding author)

requiring less restrictive assumptions than the derivation in Ref. [3]. Furthermore, the Vlasov-based MTFs allow for modeling of the full diffusion driven by noise and wakefields, not only the almost unstable modes.

2 Vlasov equation

This section introduces the Vlasov formalism and notation used throughout this paper. It follows closely the instructive explanation of direct Vlasov solvers in Ref. [5], which itself is based on Ref. [9].

The beam will in general be described by a distribution function $\Psi(x, x', y, y', z, \delta; t)$, and the single-particle dynamics are governed by an effective Hamiltonian $\mathcal{H}(x, x', y, y', z, \delta; t)$, both dependent on the phase space coordinates (x, x') in the horizontal plane, (y, y') in the vertical plane, and (z, δ) in the longitudinal plane. The vertical and longitudinal phase space coordinates can be expressed in terms of the corresponding action angle coordinates as

$$y = \sqrt{2J_y\beta_y}\cos(\theta_y), \qquad\qquad y' = \sqrt{\frac{2J_y}{\beta_y}}\sin(\theta_y), \tag{1}$$

$$z = \sqrt{2J_z\beta_z}\cos(\phi), \qquad\qquad \delta \equiv \frac{\Delta p_z}{p_0} = \sqrt{\frac{2J_z}{\beta_z}}\sin(\phi), \tag{2}$$

where β_y is an effective vertical beta function, corresponding to R/Q_{y0} in Ref. [5], β_z is an effective longitudinal beta function, corresponding to $\eta_s R/Q_s = \eta_s v/\omega_s$ in Ref. [5], $p_0 = \gamma m_0 v$ is the longitudinal momentum of the synchronous particle, R is the average radius of the circular machine, Q_{y0} is the unperturbed vertical tune, Q_s is the synchrotron tune, $\omega_s = \omega_0 Q_s$ is the synchrotron frequency, ω_0 is the (angular) rotation frequency of the beam around the machine, η_s is the slippage factor, v is the speed of the synchronous particle, γ is the relativistic factor, and m_0 is the mass of the synchronous particle. By convention, the transverse angles are written as θ_x and θ_y, while the longitudinal angle is written ϕ. The horizontal phase space coordinates (x, x') can be expressed as in Eq. (1) with all instances of y changed to x.

The evolution of the distribution Ψ due to the dynamics described by $\mathcal{H}$ is governed by the Vlasov equation

$$\frac{d\Psi}{dt} = \left(\frac{\partial}{\partial t} + \dot{\theta}_x\frac{\partial}{\partial\theta_x} + \dot{J}_x\frac{\partial}{\partial J_x} + \dot{\theta}_y\frac{\partial}{\partial\theta_y} + \dot{J}_y\frac{\partial}{\partial J_y} + \dot{\phi}\frac{\partial}{\partial\phi} + \dot{J}_z\frac{\partial}{\partial J_z}\right)\Psi = 0, \tag{3}$$

where the time evolution for this Hamiltonian system is governed by Hamilton's equations

$$\dot{J}_y \equiv \frac{dJ_y}{dt} = \frac{\partial\mathcal{H}}{\partial\theta_y}, \qquad\qquad \dot{\theta}_y \equiv \frac{d\theta_y}{dt} = -\frac{\partial\mathcal{H}}{\partial J_y}, \tag{4}$$

$$\dot{J}_z \equiv \frac{dJ_z}{dt} = \frac{\partial\mathcal{H}}{\partial\phi}, \qquad\qquad \dot{\phi} \equiv \frac{d\phi}{dt} = -\frac{\partial\mathcal{H}}{\partial J_z}. \tag{5}$$

The Vlasov equation is typically solved using perturbation theory, assuming that the Hamiltonian $\mathcal{H} = \mathcal{H}_0 + \Delta\mathcal{H}$ can be written as the sum of an unperturbed part $\mathcal{H}_0$, which here will express the focusing of the particles around the design orbit, and a first-order perturbation $\Delta\mathcal{H}$, which expresses the weak forces due to, e.g., wakefields or noise

$$\mathcal{H}_0 = \omega_0(Q_{x0} + Q'_x\delta)J_x + \omega_0(Q_{y0} + Q'_y\delta)J_y - \omega_s J_z \tag{6}$$
$$= \omega_0 Q_x J_x + \omega_0 Q_y J_y - \omega_s J_z,$$

$$\Delta\mathcal{H} = -y\frac{F_y^{\mathrm{coh}}(z; t)}{p_0} = -\sqrt{2J_y\beta_y}\cos(\theta_y)\frac{F_y^{\mathrm{coh}}(z; t)}{p_0}, \tag{7}$$

where Q_{y0} and Q'_y are the unperturbed betatron tune and linear chromaticity, respectively, in the vertical plane, and Q_{x0} and Q'_x are the equivalents in the horizontal plane. Here, it has been expressly stated that the vertical coherent force F_y^{coh} only depends on the longitudinal position and time. Hence, this formalism cannot study effects due to, e.g., beam–beam interactions, but it is sufficient for our study of dipolar wakefields and noise. Note that our derivation considers a vertical coherent force, while all results will focus on noise and wakefields in the horizontal plane.

Within such a perturbation formalism, also the distribution $\Psi = \Psi_0 + \Delta\Psi$ can be treated as the sum of an initial equilibrium part Ψ_0 and a first-order perturbation $\Delta\Psi$. The constant equilibrium distribution can be given as

$$\Psi_0 = f_0(J_x, J_y)g_0(J_z), \tag{8}$$

dependent only on the invariants of the unperturbed motion, being the actions. The dependence of $\mathcal{H}_0$ on ϕ through $Q'\delta$ is negligible [5]. Due to negligible coupling between the transverse planes and the longitudinal plane, the equilibrium distribution is separated in

the transverse and longitudinal distribution functions f_0 and g_0, respectively. The equilibrium distribution is here normalized such that

$$\int_0^{2\pi} d\theta_x \int_0^\infty dJ_x \int_0^{2\pi} d\theta_y \int_0^\infty dJ_y f_0(J_x, J_y) = 1, \tag{9}$$

$$\int_0^{2\pi} d\phi \int_0^\infty dJ_z g_0(J_z) = 1. \tag{10}$$

The goal of this derivation is to arrive at an expression for the distribution perturbation $\Delta\Psi$. Since $\Delta\mathcal{H}$ depends on y and z, $\Delta\Psi$ depends on θ_y and ϕ, as well as all the actions, but not θ_x. The linearized Vlasov equation can now be found by only keeping the terms in Eq. (3) that are linear in the perturbations of the distribution and Hamiltonian as

$$\frac{\partial \Delta\Psi}{\partial t} - \omega_0 Q_y \frac{\partial \Delta\Psi}{\partial \theta_y} + \omega_s \frac{\partial \Delta\Psi}{\partial \phi} = -\frac{\partial f_0}{\partial J_y} g_0 \sqrt{2J_y\beta_y} \sin(\theta_y) \frac{F_y^{\text{coh}}}{p_0}, \tag{11}$$

where it has been assumed that the derivatives of $\Delta\mathcal{H}$ with respect to the longitudinal action and angle are negligible. Because the coherent force is only in the vertical plane, the horizontal coordinates do not enter at this point. To solve for the distribution perturbation, we first assume that it consists of a single oscillation mode with a complex angular frequency Ω close to $\omega_0 Q_{y0}$. By making a Fourier expansion in ϕ, it can be shown that the distribution perturbation is given by (Eq. (68) in Ref. [5])

$$\Delta\Psi = e^{i\Omega t} \frac{\partial f_0}{\partial J_y} \sqrt{2J_y\beta_y} e^{i\theta_y} e^{-\frac{iQ_y' z}{Q_s\beta_z}} \sum_{l=-\infty}^\infty R_l(J_z) e^{-il\phi}, \tag{12}$$

where $Q_y' z / Q_s \beta_z$ is the headtail phase factor due to chromaticity. The transverse part of the distribution perturbation is fully specified. The longitudinal distribution perturbation consist of the Fourier sum over the so far unspecified functions $R_l(J_z)$, which can be found by solving the linearized Vlasov equation that now takes form (Eq. (69) in Ref. [5])

$$\sum_{l=-\infty}^\infty R_l(J_z) e^{-il\phi} (\Omega - \omega_0 Q_{y0} - l\omega_s) = e^{-i\Omega t} e^{\frac{iQ_y' z}{Q_s\beta_z}} g_0(J_z) \frac{F_y^{\text{coh}}}{2p_0}. \tag{13}$$

In the following, we will interchangeably use the radial coordinate $r_z = \sqrt{2J_z\beta_z}$ to simplify the notation and analytical calculations. This change of coordinate is not used when expressing Hamilton's equations; hence, it does not need to be a canonical transformation [10].

3 Beam transfer function

A transfer function of a system represents the relationship between the output signal and the input signal. The transverse beam transfer function (BTF) typically represents the relationship between the transverse oscillation amplitude of the center of mass of the beam (output) and the excitation signal provided by magnets (input) [6–8]. The excitation signal can either be broadband or consists of a single frequency.

3.1 Beam transfer function with chromaticity

First, we want to derive an expression for the BTF including chromaticity. We consider the coherent force F_y^{coh} to be an external harmonic driving force of amplitude A_y and frequency Ω

$$F_y^{\text{coh}}(z, t) = A_y e^{i\Omega t}. \tag{14}$$

Putting it in Eq. (13) and using the Jacobi–Anger expansion (Eq. (8.511.4) in Ref. [11]) give

$$\sum_{l=-\infty}^\infty R_l(r_z) e^{-il\phi} (\Omega - \omega_0 Q_{y0} - l\omega_s) = \frac{A_y}{2p_0} g_0(r_z) \sum_{l=-\infty}^\infty i^l e^{il\phi} J_l\left(\frac{Q_y' r_z}{Q_s\beta_z}\right), \tag{15}$$

where $J_l(\cdot)$ are the Bessel functions of order l. By equating terms with $e^{-il\phi}$, one gets an expression for the longitudinal modes

$$R_l(r_z) e^{-il\phi} = \frac{A_y}{2p_0} \frac{g_0(r_z)}{\Omega - \omega_0 Q_{y0} - l\omega_s} i^{-l} e^{-il\phi} J_{-l}\left(\frac{Q_y' r_z}{Q_s\beta_z}\right). \tag{16}$$

Inserting this into the expression for the distribution perturbation in Eq. (12) gives

$$\Delta\Psi = \frac{A_y}{2p_0}e^{i\Omega t}e^{i\theta_y}\frac{\partial f_0}{\partial J_y}g_0(r_z)\sqrt{2J_y\beta_y}\sum_{k,l}\frac{i^{l-k}e^{i(k-l)\phi}}{\Omega-\omega_0 Q_y(J_x,J_y)-l\omega_s}J_k\left(\frac{Q'_y r_z}{Q_s\beta_z}\right)J_l\left(\frac{Q'_y r_z}{Q_s\beta_z}\right), \tag{17}$$

where we have introduced a weak transverse detuning that is a function of the transverse actions as in Ref. [6], such as the detuning driven by octupole magnets [12]

$$Q_y(J_x,J_y) = Q_{0y} + a_y J_y + b_y J_x. \tag{18}$$

We are now in a position to calculate the BTF, defined as the beam response to the driving force. By realizing that only terms with $k=l$ do not vanish when integrating $\Delta\Psi$ over ϕ and that the equilibrium distribution is normalized as in Eqs. (9) and (10), one finds

$$\begin{aligned}
\mathrm{BTF} &\equiv \frac{y^{\mathrm{dip}}}{F_y^{\mathrm{coh}}}\frac{p_0}{\beta_y} \equiv \frac{p_0}{F_y^{\mathrm{coh}}\beta_y}\frac{\int_0^{2\pi}\mathrm{d}\theta_x\int_0^\infty \mathrm{d}J_x\int_0^{2\pi}\mathrm{d}\theta_y\int_0^\infty \mathrm{d}J_y\int_0^{2\pi}\mathrm{d}\phi\int_0^\infty \mathrm{d}J_z(\Psi_0+\Delta\Psi)\sqrt{2J_y\beta_y}\cos(\theta_y)}{\int_0^{2\pi}\mathrm{d}\theta_x\int_0^\infty \mathrm{d}J_x\int_0^{2\pi}\mathrm{d}\theta_y\int_0^\infty \mathrm{d}J_y\int_0^{2\pi}\mathrm{d}\phi\int_0^\infty \mathrm{d}J_z(\Psi_0+\Delta\Psi)} \\
&= 4\pi^3\sum_{l=-\infty}^{\infty}\int_0^\infty\int_0^\infty\frac{J_y\dfrac{\partial f_0}{\partial J_y}}{\Omega-\omega_0 Q_y(J_x,J_y)-l\omega_s}\mathrm{d}J_x\mathrm{d}J_y\int_0^\infty J_l\left(\frac{Q'_y r_z}{Q_s\beta_z}\right)^2 g_0(r_z)\frac{r_z\mathrm{d}r_z}{\beta_z},
\end{aligned} \tag{19}$$

where y^{dip} is the dipolar moment of the bunch. The dipolar moment is scaled by the beta function β_y so that it is given in terms of y', as seen in Eq. (1). The force is scaled by the momentum p_0, as in Eq. (34) in Ref. [5], to be the change of y'. The BTF can be put in the form

$$\mathrm{BTF} = \sum_l \mathcal{T}_l(\Omega)w_{0l}(Q'_y), \tag{20}$$

with the familiar dispersion integral [6] and a weight that depends on chromaticity

$$\mathcal{T}_l(\Omega) \equiv 2\pi^2\int_0^\infty\int_0^\infty\frac{J_y\dfrac{\partial f_0}{\partial J_y}}{\Omega-\omega_0 Q_y(J_x,J_y)-l\omega_s}\mathrm{d}J_x\mathrm{d}J_y, \tag{21}$$

$$w_{0l}(Q'_y) \equiv 2\pi\int_0^\infty J_l\left(\frac{Q'_y r_z}{Q_s\beta_z}\right)^2 g_0(r_z)\frac{r_z\mathrm{d}r_z}{\beta_z}. \tag{22}$$

In the absence of chromaticity, w_{0l} is 1 for $l=0$ and 0 otherwise, returning $\mathcal{T}_0$ as the BTF. For a Gaussian distribution with variation $\sigma_z^2 = \langle J_z\beta_z\rangle$ and use of Eq. (6.633) in Ref. [11], we recover the result in Ref. [8]

$$g_0(r_z) = \frac{\beta_z}{2\pi\sigma_z^2}e^{-\frac{r_z^2}{2\sigma_z^2}}, \qquad\qquad w_{0l}^G(Q'_y) = e^{-\left(\frac{Q'_y\sigma_z}{Q_s\beta_z}\right)^2}I_l\left(\left(\frac{Q'_y\sigma_z}{Q_s\beta_z}\right)^2\right), \tag{23}$$

where $I_l(\cdot)$ are the modified Bessel functions of the first kind.

3.2 Wakefield beam eigenmode transfer function

In Sect. 3.1, we considered the coherent driving force in Eq. (14) with beam-independent amplitude. Now, we will study the driving by the coherent wake force F_y^{wake}, which depends on the transverse beam motion. In the following, we adopt the weak wakefield approximation, assuming that the beam modes of different azimuthal number l are linearly independent. To distinguish between different modes, we introduce the subscript m, such that mode m has azimuthal number l_m and so forth. Note that different modes $m\neq n$ can have the same azimuthal mode number $l_m = l_n$, but a particular mode has only a single l_m. For ease of notation, the longitudinal polar radius $r_z = \sqrt{2J_z\beta_z}$ is used instead of the longitudinal action.

The wake force due to the passings of a beam eigenmode at all turns k can be given as (Eq. (85) in Ref. [5])

$$F_{ym}^{\mathrm{wake}}(z;t) = e^{i\Omega_m t}\frac{i^{1+l_m}Ne^2\omega_0}{2\pi\beta_z Q_{y0}}\sum_{k=-\infty}^{\infty}Z_y(\Omega_m+k\omega_0)e^{-i(\Omega_m+k\omega_0)\frac{z}{v}}\mathcal{I}_{l_m k}, \tag{24}$$

$$\mathcal{I}_{l_m k} = \int_0^\infty R_{l_m}(r'_z)J_{l_m}\left[\left(\Omega_m+k\omega_0-\frac{Q'_y v}{Q_s\beta_z}\right)\frac{r'_z}{v}\right]r'_z\mathrm{d}r'_z, \tag{25}$$

where Z_y is the impedance function, *i.e.* the Fourier transform of the wake function, and N is the number of particles in the bunch. With this expression for the coherent force, Sacherer's integral equation [13] takes the form (Eq. (88) in Ref. [5])

$$
\begin{aligned}
& R_{l_m}(r_z)(\Omega_m - \omega_0 Q_{y0} - l_m \omega_s) \\
& = g_0(r_z) \frac{i N e^2 \omega_0}{4\pi \beta_z Q_{y0} p_0} \sum_{k=-\infty}^{\infty} Z_y(\Omega_m + k\omega_0) J_{l_m} \left[\left(\Omega_m + k\omega_0 - \frac{Q'_y v}{Q_s \beta_z} \right) \frac{r_z}{v} \right] \mathcal{I}_{l_m k},
\end{aligned}
\tag{26}
$$

where it has been used that the modes have a single azimuthal mode number l_m. This set of equations can be solved numerically with direct Vlasov solvers, such as DELPHI [14], to find the transverse eigenmodes $\Delta\Psi_m$ and their frequencies Ω_m. These mode details can also be found using codes that implement the circulant matrix model, such as BimBim [15]. Both these codes have been used in this paper.

The wake force due to a dipolar eigenmode is often expressed as proportional to the dipolar transverse offset, $F_y^{\mathrm{wake}}/p_0 = -2\Delta\Omega\langle y\rangle/\beta_y$ [6], where $\Delta\Omega$ is the tune shift driven by the wakefields. The factor β_y/p_0 occurs here as in Eq. (19) to properly scale the force to the change of position, as in Ref. [5]. Here, we aim at generalizing this proportionality of the wake force for an eigenmode with transverse offset dependent on the longitudinal phase space. To that end, we calculate the transverse offset of the mode as a function of the longitudinal coordinates

$$
\begin{aligned}
\langle y(r_z, \phi; t)\rangle_m &= \frac{\int_0^{2\pi} d\theta_x \int_0^\infty dJ_x \int_0^{2\pi} d\theta_y \int_0^\infty dJ_y \sqrt{2J_y \beta_y} \cos(\theta_y)(\Psi_0 + \Delta\Psi_m)}{\int_0^{2\pi} d\theta_x \int_0^\infty dJ_x \int_0^{2\pi} d\theta_y \int_0^\infty dJ_y (\Psi_0 + \Delta\Psi_m)} \\
&= -\frac{\beta_y}{g_0(r_z)} e^{i\Omega_m t} e^{-\frac{i Q'_y z}{Q_s \beta_z}} R_{l_m}(r_z) e^{-i l_m \phi},
\end{aligned}
\tag{27}
$$

where it has been used that the average offset due to the equilibrium distribution Ψ_0 in the numerator is 0 and the integral over the wakefield eigenmode $\Delta\Psi_m$ in the denominator is 0.

In general, there does not exist a scalar proportionality constant between $F_{ym}^{\mathrm{wake}}(z; t)$ and $\langle y(r_z, \phi; t)\rangle_m$ at any given instant of time, since the former depends only on z, while the latter depends on both r_z and ϕ. However, by combining Eqs. (24)–(27), one can find that

$$
\frac{\beta_y}{p_0} \left\langle \frac{F_{ym}^{\mathrm{wake}}(z; t)}{\langle y(r_z, \phi; t)\rangle_m} \right\rangle_t = -2(\Omega_m - \omega_0 Q_{y0} - l_m \omega_s) \equiv -2\Delta\Omega_m,
\tag{28}
$$

where the time average of the ratio is taken over one synchrotron period $\tau_s = 1/\omega_s$. This time averaging corresponds to an averaging over the longitudinal phase ϕ, which also enters in z as given by Eq. (2). Therefore, we suggest instead an effective force, as in Ref. [3], that is proportional to the transverse offset, including its dependence on the longitudinal coordinates

$$
F_{ym}^{\mathrm{wake\,eff}}(r_z, \phi; t) = -\frac{2p_0}{\beta_y} \Delta\Omega_m \langle y(r_z, \phi; t)\rangle_m.
\tag{29}
$$

A noise force acting on the beam is now introduced in addition to the wake force

$$
F_y^{\mathrm{noise}} = \frac{p_0}{\beta_y} \xi(z; t).
\tag{30}
$$

Since the noise does not depend on the beam, it is not expected to change the shape of the wakefield beam eigenmodes $\Delta\Psi_m$. However, it will excite more than one mode at once. Hence, we can no longer consider a single wakefield beam eigenmode. Instead, we get

$$
\Delta\Psi = \Delta\Psi_m \qquad\qquad \rightarrow \qquad\qquad \Delta\Psi = \sum_m \Delta\Psi_m,
\tag{31}
$$

$$
\langle y(r_z, \phi; t)\rangle = \langle y(r_z, \phi; t)\rangle_m \qquad \rightarrow \qquad \langle y(r_z, \phi; t)\rangle = \sum_m \langle y(r_z, \phi; t)\rangle_m \equiv \sum_m \chi_m(t) m_m(r_z, \phi),
\tag{32}
$$

where we have introduced as in Ref. [3] the time-dependent mode amplitude $\chi_m(t)$ and normalized constant eigenmode shape functions $m_m(r_z, \phi)$, which by comparison to Eq. (27) can be found to be

$$
m_m(r_z, \phi) = A_m e^{-\frac{i Q'_y z}{Q_s \beta_z}} \frac{R_{l_m}(r_z)}{g_0(r_z)} e^{-i l_m \phi},
\tag{33}
$$

where A_m is a normalization constant such that

$$
\langle m_m^* m_m \rangle_z \equiv \int_0^{2\pi} d\phi \int_0^\infty dJ_z m_m^* m_m g_0 = 1,
\tag{34}
$$

where the superscripted $*$ implies a complex conjugation and it has been used that g_0 is normalized, as given by Eq. (10). Note that the average over the longitudinal coordinates, denoted by $\langle \cdot \rangle_z$, includes the unperturbed longitudinal distribution g_0 in the integrand. These excited modes are not necessarily orthogonal, but are still assumed to be linearly independent and can therefore be treated independently.

The noise can be modeled as a single kick per particle per turn. The noise signal $\xi(z; t)$ can be decomposed in orthonormal noise shape functions $\Xi_i(z)$, which are polynomials of order i, being $\Xi_0 = 1$, $\Xi_1 = z/\sigma_z$, and higher-order polynomials for a longitudinally Gaussian distribution. These noise shape functions can themselves be decomposed in the eigenmode shape functions m_m

$$\xi(z; t) = \sum_i \xi_i(t) \Xi_i(z) = \sum_i \xi_i(t) \sum_m \eta_{i\,m} m_m(r_z, \phi), \tag{35}$$

where the noise signals $\xi_i(t)$ are assumed to only have power in positive frequencies $\omega \in [0, \omega_0/2)$ and the noise-mode moments $\eta_{i\,m}$ are the projection coefficients of the noise shape function Ξ_i on the mode shape function m_m. The noise shape functions are normalized over the initial equilibrium distribution function as

$$\langle \Xi_i^* \Xi_j \rangle_z = \sum_m \eta_{i\,m}^* \langle m_m^* \Xi_j \rangle_z \equiv \sum_m \eta_{i\,m}^* \tilde{\eta}_{j\,m} = \delta_{i,j}, \tag{36}$$

where $\delta_{i,j}$ is the Kronecker delta and $\tilde{\eta}_{j\,m} \equiv \langle m_m^* \Xi_j \rangle_z$ is equal to $\eta_{j\,m}$ if the modes are orthogonal. If not, $\eta_{j\,m}$ can be found by solving a linear system of equations. Most noise sources produce noise that is constant across a bunch, being proportional to the constant $\Xi_0(z) = 1$. This type of noise will be referred to as rigid or dipolar noise. The shape of crab cavity amplitude noise, on the other hand, is proportional to the longitudinal position, $\Xi_1(z) \propto z$. To the authors' knowledge, there are no significant noise sources for which higher-order terms in z are necessary.

The full coherent force can now be decomposed as:

$$\begin{aligned} F_y^{\text{coh}} &= F_y^{\text{wake eff}} + F_y^{\text{noise}} \\ &= \frac{p_0}{\beta_y} \sum_m \left(-2\Delta\Omega_m \chi_m(t) + \sum_i \xi_i(t) \eta_{i\,m} \right) m_m(r_z, \phi) \\ &\equiv \sum_m F_{y\,m}^{\text{coh}}, \end{aligned} \tag{37}$$

where the coherent force $F_{y\,m}^{\text{coh}}$ proportional to mode m has been defined.

To get the transfer function of mode m, one must now calculate the expected excitation due to noise at a given driving frequency Ω. The mode is then forced to oscillate at the driving frequency, even if it is different from the natural eigenfrequency of a mode Ω_m. In general, the closer the driving frequency is to the eigenfrequency, the larger the amplitude of the modes motion is expected to be. By combining Eqs. (12) and (13) with the assumption of a single azimuthal mode number l_m per linearly independent mode, meaning that the sums over l are exchanged for a single term, one gets the expression

$$\Delta\Psi_m = \frac{\sqrt{2J_y \beta_y} e^{i\theta_y} \frac{\partial \Psi_0}{\partial J_y}}{\Omega - \omega_0 Q_y(J_x, J_y) - l_m \omega_s} \frac{F_{y\,m}^{\text{coh}}}{2p_0}, \tag{38}$$

where we have again introduced a weak transverse detuning. The average offset of mode m at frequency Ω can be calculated with the first line of Eqs. (27) and (38)

$$\begin{aligned} \langle y(r_z, \phi; t) \rangle_m &= \chi_m(t) m_m(r_z, \phi) \\ &= \mathcal{T}_{l_m}(\Omega) \left(-2\Delta\Omega_m \chi_m(t) + \sum_i \xi_i(t) \eta_{i\,m} \right) m_m(r_z, \phi), \end{aligned} \tag{39}$$

where the dispersion integral $\mathcal{T}_{l_m}(\Omega)$ in Eq. (21) has reappeared. By rearranging the terms, we get an expression for the wakefield beam eigenmode transfer function (MTF) due to the excitation by noise at frequency Ω

$$\frac{\hat{\chi}_m(\Omega)}{\sum_i \hat{\xi}_i(\Omega) \eta_{i\,m}} = \frac{\mathcal{T}_{l_m}(\Omega)}{1 + 2\Delta\Omega_m \mathcal{T}_{l_m}(\Omega)} = \frac{1/2}{\Delta\Omega_m - \Delta\Omega_{l_m}^{\text{SD}}(\Omega)} \equiv \mathcal{T}_{l_m}^{\text{wake}}(\Omega), \tag{40}$$

where the notation $\hat{f}(\Omega) \equiv \int_{-\infty}^{\infty} f(t) \exp(-i\Omega t) \mathrm{d}t$ indicates the Fourier transform of $f(t)$. The amplitude of mode m diverges when $\Delta\Omega_m \to -1/[2\mathcal{T}_{l_m}(\Omega)] = \Delta\Omega_{l_m}^{\text{SD}}(\Omega)$. $\Delta\Omega_{l_m}^{\text{SD}}(\Omega)$ is an important quantity in beam stability, often referred to as the stability diagram. Examples of the stability diagram are illustrated in Fig. 6. A mode is considered to be stabilized by Landau damping when its complex tune is inside (below) the stability diagram [6]. Note also the appearance of $\eta_{i\,m}$ in the summand in the denominator on
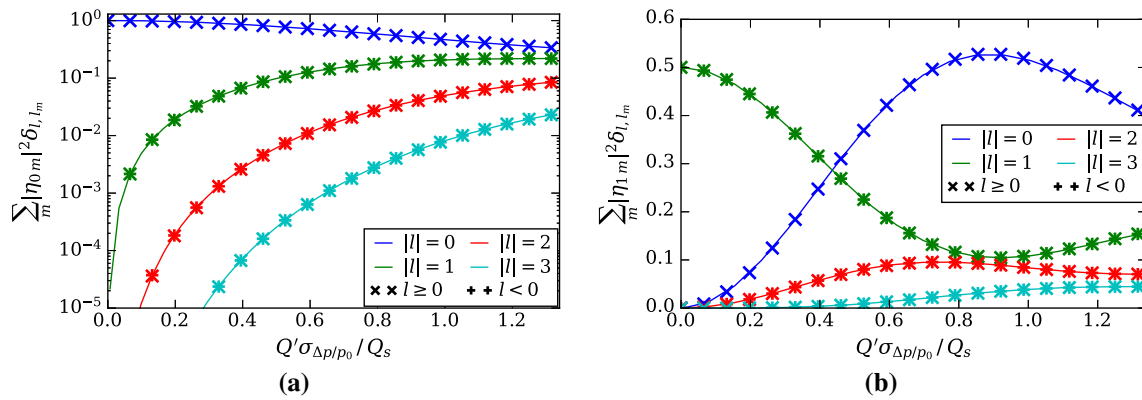
Fig. 1 Weights of low-order sidebands of the BTF. In (**a**) rigid motion due to rigid noise $\propto \varXi_0$. In (**b**) headtail motion due to headtail noise $\propto \varXi_1$. The fully analytical theories (lines) in Eqs. (22) and (B.7) are compared to the MTF theory (points) in Eqs. (44) and (B.10), based on DELPHI calculations and assuming orthonormal modes

the left-hand side. A smaller value of $\eta_{i\,m}$ means that the noise ξ_i is less effective at exciting mode m. The combined coherent force from the noise and wakefields related to mode m in Eq. (37) can with this MTF be expressed as:

$$\hat{F}_{y\,m}^{\text{coh}} = \frac{p_0}{\beta_y} \frac{\sum_i \hat{\xi}_i(\Omega) \eta_{i\,m}}{1 + 2\Delta\Omega_m \mathcal{T}_{l_m}(\Omega)} m_m(r_z, \phi). \tag{41}$$

3.3 Beam transfer function including wakefields

The MTF for a single linearly independent beam mode with a single azimuthal mode number l_m is given in Eq. (40). To express the measurable dipolar BTF, the MTF of all modes must be combined. Since the BTF typically is measured by controlled excitation by a dipolar noise source, which excites all particles in the bunch equally, we will in this section assume that $\xi_0(t)$ is the only noise signal of nonzero amplitude.

The dipolar mode moment can be calculated as

$$y_m^{\text{dip}}(t) = \chi_m \langle m_m \rangle_z = \chi_m \langle \varXi_0^* m_m \rangle_z = \chi_m \tilde{\eta}_{0\,m}^*, \tag{42}$$

where it was used that $\varXi_0(z) = 1$. By combining with Eq. (40), and assuming only dipolar noise, we get the desired expression for the BTF including wakefields

$$\text{BTF} = \frac{\hat{y}^{\text{dip}}}{\hat{F}_y^{\text{noise}}} \frac{p_0}{\beta_y} = \frac{\hat{y}^{\text{dip}}(\Omega)}{\hat{\xi}_0(\Omega)} = \frac{\sum_m \hat{y}_m^{\text{dip}}(\Omega)}{\hat{\xi}_0(\Omega)} = \sum_m \mathcal{T}_{l_m}^{\text{wake}}(\Omega) \tilde{\eta}_{0\,m}^* \eta_{0\,m}, \tag{43}$$

where F_y^{noise} is defined in Eq. (30) and $\mathcal{T}_{l_m}^{\text{wake}}(\Omega)$ is defined in Eq. (40). In the absence of chromaticity and wakefields, Eq. (43) returns the standard BTF, $\mathcal{T}_0(\Omega)$. In the limit of negligible wakefields, but still including chromaticity, such that $\mathcal{T}_{l_m}^{\text{wake}} = \mathcal{T}_{l_m}$, we can by comparison to Eq. (20) calculate the weight of sideband l as

$$w_{0l}^{\text{MTF}} = \sum_m \tilde{\eta}_{0\,m}^* \eta_{0\,m} \delta_{l,l_m}. \tag{44}$$

The weight w_{0l}^{MTF} is, in the limit of negligible wakefields, equivalent to the weight w_{0l} in Eq. (22), which was derived in the presence of chromaticity but completely without wakefields.

So far, the derivation has not made any assumptions as to the orthogonality of the modes, leading to the distinction between $\tilde{\eta}$ and η in Eq. (44). If the modes are orthogonal, one has $\tilde{\eta}_{0\,m}^* \eta_{0\,m} = |\eta_{0\,m}|^2$. This has been found to be true within the numerical accuracy of BimBim for the LHC.

The weights w_{0l} in Eq. (22) and the weights w_{0l}^{MTF} in Eq. (44), assuming orthogonal modes and using negligible wakefields in DELPHI, are compared in Fig. 1a. This figure shows how the dipolar moment of modes with nonzero azimuthal mode number $l_m \neq 0$ increases with the chromaticity, a behavior that is important for the mechanisms in this paper. How the weights are calculated in DELPHI is explained in Appendix A.

One can alternatively imagine a headtail BTF (BTF$^{\text{ht}}$), excited by headtail noise $\propto \varXi_1$ whereupon the headtail motion is measured. This is further explained and derived in Appendix B. The theoretical weights w_{1l} in Eq. (B.7) are in Fig. 1b compared to the weights w_{1l}^{MTF} in Eq. (B.10), assuming orthogonal modes. This figure shows how crab cavity amplitude noise can efficiently excite modes of azimuthal mode number $l_m = \pm 1$ at small chromaticities.
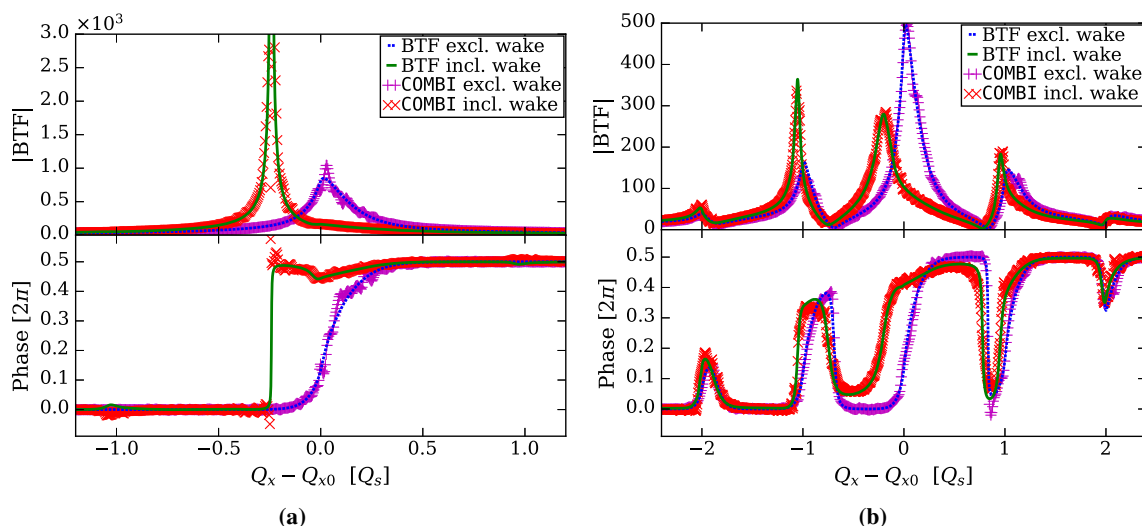
Fig. 2 BTF in the horizontal plane without chromaticity in (**a**) and with a linear chromaticity of $Q'_x = 15$ in (**b**). In both cases, multi-particle simulations run with COMBI are compared to the BTF excluding wakefields in Eq. (20) and the BTF including wakefields in Eq. (43). The BTFs including wakefields were calculated based on BimBim calculations

3.4 Comparison to multi-particle tracking simulations

The expressions derived for the BTF in Eqs. (20) and (43) will here be benchmarked against multi-particle tracking simulations run with COMBI [16,17]. Calculations made with BimBim, using the impedance model for the LHC at top energy in 2018, have been used to get the mode details required by Eq. (43), *i.e.* the noise-mode-moments η_{0m} and tune shifts ΔQ_m^{coh}. The bunch intensity, synchrotron tune, and root-mean-squared (rms) particle momentum spread were the same as given by Table 1, see below. The tracking simulations were run with 10^7 macro-particles for 10^5 turns, from which the BTF was found by calculating the power spectral density of the beam signal and noise using the Welch algorithm. The horizontal noise used was approximately white with an rms kick per turn of $5 \times 10^{-4}\sigma_x$, in units of the beam size.

The new theories and the tracking simulations, both with and without wakefields, show excellent agreement in Fig. 2. It is clearly shown that it is the wakefields in the LHC that cause the shift of the main peak (and side peaks as well) of the BTF, as has been hypothesized based on measurements in the LHC (Fig. 7 in Ref. [7]). Although it is not shown here visually, the theory in Eq. (20) is also able to explain the appearance of loops at the sidebands in the stability diagram reconstructed based on the BTF [18].

4 Loss of Landau damping driven by diffusion

Instabilities have been observed in the LHC that occur after a long latency, in the order of tens of minutes, after reaching top energy. The mechanism behind these instabilities has just recently been understood [3]: the interplay between noise and wakefields drives a diffusion that eventually renders the beam unstable. In Ref. [3], the expression for the diffusion was based on the MTF for a mode modeled as a single underdamped stochastic harmonic oscillator (USHO). In this section, we will derive the diffusion by use of the MTF in Eq. (40), which is based on the linear Vlasov theory. The new derivation was inspired by the second part of Ref. [19], yet relaxing strong assumptions that prevented quantitative estimates for realistic machines. Most important was to relax the rigid bunch assumption and the simplified wakefield model, which corresponded to only considering mode shape functions m_m that were independent of the longitudinal coordinates r_z and ϕ. In addition, we have extended from using a one-dimensional tune spread, setting b_y in Eq. (18) to 0, to using a two-dimensional tune-spread. The new Vlasov theory will be compared to the existing USHO theory.

4.1 Diffusion driven by wakefield eigenmodes

If the vertical noise and wakefields are sufficiently weak to be modeled as a perturbation, they drive a second-order diffusion of the equilibrium distribution. This requires a limited change of the distribution over the correlation period of the coherent force. The

diffusion in the vertical plane can be modeled analytically by [20,21]

$$\frac{\partial \Psi_{\text{eq}}}{\partial t} = \frac{\partial}{\partial J_y}\left[J_y D_y \frac{\partial \Psi_{\text{eq}}}{\partial J_y}\right], \tag{45}$$

$$D_y = \lim_{T \to \infty}\frac{1}{T}\int\limits_{t_0}^{t_0+T}\mathrm{d}t\int\limits_{t_0}^{t_0+T}\mathrm{d}s\,\frac{\left\langle \dot{J}_y(t)\dot{J}_y(s)\right\rangle_z}{2J_y}, \tag{46}$$

where the equilibrium distribution has been renamed $\Psi_0 \to \Psi_{\text{eq}}$ since it will evolve with time. The autocorrelation of the change of action is averaged over the longitudinal coordinates, as how the transverse diffusion depends on the longitudinal action is irrelevant. An equivalent horizontal diffusion term can be added to Eq. (45) to model the diffusion driven by horizontal noise and wakefields. There is assumed no coupling between the two transverse planes in terms of diffusion.

Since the wake force in Eq. (24) is complex, it will give a complex expression for $\dot{J}_y$ by use of Eq. (4). Therefore, we calculate a real expression for the change of action as

$$\dot{J}_y(t) = 2\mathrm{Re}\left\{\frac{\partial \Delta \mathcal{H}}{\partial \theta_y}\right\} = -\frac{\sqrt{2J_y\beta_y}}{p_0}\mathrm{Re}\left\{ i\left(\mathrm{e}^{i\theta_y(t)} - \mathrm{e}^{-i\theta_y(t)}\right)\sum_m F_{ym}^{\text{coh}}(r_z, \phi + \omega_s t; t)\right\}, \tag{47}$$

where θ_y is the angle of the single particle. It can be shown as in Ref. [3] that the vertical single particle angle is

$$\theta_y = \theta_{0y} - \omega_0 Q_y t + \frac{Q'_y z}{Q_s \beta_z}. \tag{48}$$

Since $F_{ym}^{\text{wake}} \propto \exp(i\Omega t)$, with $\Omega \sim \Omega_m$, and F^{noise} is assumed to only have power in positive frequencies, only the close-to-resonant term $\exp(i\theta_y) \propto \exp(-i\omega_0 Q_y t)$ will give a nonnegligible integrated change of action. The headtail phase factor $Q'_y z/Q_s\beta_z$ in the single particle angle θ_y in Eq. (47) will then cancel the headtail phase factor of the coherent force in Eq. (37), contained within the functions m_m in (33). Note that as we are no longer focused on the behavior of the modes, but rather on their consequences on the individual particles, we are now referring to $\omega_y \sim \omega_0 Q_{y0}$, the frequencies of the individual particles, instead of $\Omega_m \sim \omega_0 Q_{y0} + l_m\omega_s$, the frequency of the mode.

The integrand in Eq. (46), neglecting the averaging over z, becomes

$$\begin{aligned}\frac{\dot{J}_y(t)\dot{J}_y(s)}{2J_y} &= \frac{-\beta_y}{4p_0^2}\left[\mathrm{e}^{i(\theta_{0y}-\omega_y t)}\sum_m F_{ym,z=0}^{\text{coh}}(\phi+\omega_s t; t) - \text{c.c.}\right]\\&\quad \times \left[\mathrm{e}^{i(\theta_{0y}-\omega_y s)}\sum_n F_{yn,z=0}^{\text{coh}}(\phi+\omega_s s; s) - \text{c.c.}\right] + \mathcal{O}(0)\\&= \frac{\beta_y}{4p_0^2}\left[\mathrm{e}^{-i\omega_y(t-s)}\sum_m F_{ym,z=0}^{\text{coh}}(0; t)\mathrm{e}^{-il_m(\phi+\omega_s t)}\sum_n F_{yn,z=0}^{\text{coh}*}(0; s)\mathrm{e}^{il_n(\phi+\omega_s s)} + \text{c.c.}\right] + \mathcal{O}(0)\\&= \frac{\beta_y}{4p_0^2}\left[\sum_m\sum_n \mathrm{e}^{-i(\omega_y+l_n\omega_s)u}F_{ym,z=0}^{\text{coh}}(0; t)F_{yn,z=0}^{\text{coh}*}(0; t-u)\mathrm{e}^{-i(l_m-l_n)(\phi+\omega_s t)} + \text{c.c.}\right] + \mathcal{O}(0), \tag{49}\end{aligned}$$

where $\omega_y = \omega_y(J_x, J_y) = \omega_0 Q_y(J_x, J_y)$ is the transverse frequencies of the individual particles, which depends on the transverse actions of the particles, the subscript $z = 0$ in $F_{ym,z=0}^{\text{coh}}$ means that the headtail factor is canceled out, both c.c. and the superscripted $*$ imply complex conjugation, $\mathcal{O}(0)$ refers to terms that later in the calculation would become 0, and the time parameter s has been exchanged for $u = t - s$. In the first line, $\mathcal{O}(0)$ refers to terms that later will become 0 due to the lack of noise in negative frequencies. In the second line, $\mathcal{O}(0)$ additionally refers to non-resonant terms proportional to $\exp[i\omega_y(s+t)]$ that will average to zero. For this reason, the factors $\exp(i\theta_{0y})$ cancel. In the second line, the dependence on the particles longitudinal phase $\phi + \omega_s t$, including how it evolves with time, is also taken out of the coherent force.

To calculate the diffusion coefficient driven by noise and noise-excited wakefields, as modeled by the Vlasov theory derived in this paper, the last line in Eq. (49) must be treated as given by Eq. (46), with s exchanged for $u = t - s$. Remember from Eq. (34) that $\langle\cdot\rangle_z$ means an averaging over both ϕ and J_z. The averaging over ϕ gives that $l_m = l_n$, i.e., that modes close to different sidebands do not interact to drive a common diffusion since they are orthogonal. The calculation then becomes the double sum of the Fourier transform of the cross-correlation function of F_{ym}^{coh} and F_{yn}^{coh}, which is the product of their Fourier transforms

$$D_y^{\text{Vlasov}}(J_x, J_y) = \frac{\beta_y}{2p_0^2}\sum_m\sum_n\left\langle \hat{F}_{ym}^{\text{coh}}(\omega_y + l_m\omega_s)\hat{F}_{yn}^{\text{coh}*}(\omega_y + l_n\omega_s)\right\rangle_z, \tag{50}$$

where a factor 2 has come from the inclusion of the complex conjugate in Eq. (49). Note that this expression is real, as it contains the sum over pairs of complex conjugated expressions. Looking at the expression for $\hat{F}_{ym}^{\text{coh}}$ in Eq. (41), we find that orthogonal modes

with $\langle m_m m_n^* \rangle = 0$ will not contribute to the diffusion coefficient. In the unperturbed case, all modes are orthogonal. Since we have adopted the hypothesis of weak wakefields, we assume that the contribution of the terms with $m \neq n$ remains negligible compared to the diagonal terms. This hypothesis was confirmed numerically in all the cases studied. Therefore, we only keep the dominant terms with $m = n$. The diffusion coefficient can finally be expressed as a function of the transverse actions as

$$D_y^{\text{Vlasov}}(J_x, J_y) = \sum_m D_{ym}^{\text{Vlasov}}[\omega_y(J_x, J_y)] = \frac{\beta_y}{2p_0^2} \sum_m \left\langle \left| \hat{F}_{ym}^{\text{coh}}(\omega_y + l_m \omega_s) \right|^2 \right\rangle_z, \tag{51}$$

$$D_{ym}^{\text{Vlasov}}(\omega_y) = \frac{\sum_i \left| \hat{\xi}_i(\omega_y + l_m \omega_s) \right|^2 |\eta_{im}|^2}{2\beta_y} \frac{\left| \Delta\Omega_{l_m}^{\text{SD}}(\omega_y + l_m \omega_s) \right|^2}{\left| \Delta\Omega_m - \Delta\Omega_{l_m}^{\text{SD}}(\omega_y + l_m \omega_s) \right|^2}. \tag{52}$$

The term $l_m \omega_s$ in the argument to $\Delta\Omega_{l_m}^{\text{SD}}$ will cancel the same term in Eq. (21). Hence, a mode with eigenfrequency Ω_m close to a sideband $\omega_0 Q_{y0} + l_m \omega_s$ can still drive diffusion of particles with betatron frequency $\omega_y \sim \omega_0 Q_{y0}$, which is far away from the sidebands. That is often the case in the LHC. Note that the noise signals ξ_i are given in units of the beam size, $\sigma_y = \sqrt{2J_y\beta_y}$, so the factors β_y will cancel.

We will now compare the new Vlasov theory to the USHO theory derived in Ref. [3]. The USHO theory assumes that the motion of the unstable mode with complex frequency shift $\Delta\Omega_m$ (with positive imaginary part) can be modeled as a single underdamped harmonic oscillator with complex frequency shift changed to $\Delta\Omega_m^{\text{LD}}$ (with negative imaginary part) when stabilized by Landau damping. If $\text{Im}\left\{\Delta\Omega_m^{\text{LD}}\right\} > 0$, the Landau damping is not sufficient to stabilize the mode. The interpretation of $\Delta\Omega_m^{\text{LD}}$ is further explained in Ref. [3]. Assuming small tune shifts, the MTF in the USHO theory is

$$\left. \frac{\hat{\chi}_m(\Omega)}{\sum_i \hat{\xi}_i(\Omega)\eta_{im}} \right|^{\text{USHO}} = \frac{1/2}{\Delta\Omega_m^{\text{LD}} - \Delta\omega_y}, \tag{53}$$

where $\Delta\omega_y = \omega_y - \omega_0 Q_{y0}$ is the frequency shift of the individual particles. Equation (53) can be compared to Eq. (40). All consequential differences originate in the different expressions for the MTFs. Assuming orthonormal mode shapes m_m, the diffusion coefficient due to both noise and wakefields according to the USHO theory (only diffusion driven by wakefields was treated in Ref. [3]) can in the notation and framework used in this paper be written as

$$D_{ym}^{\text{USHO}}(\omega_y) = \frac{\sum_i \left| \hat{\xi}_i(\omega_y + l_m \omega_s) \right|^2 |\eta_{im}|^2}{2\beta_y} \frac{\left| \Delta\Omega_m^{\text{LD}} - \Delta\omega_y - \Delta\Omega_m \right|^2}{\left| \Delta\Omega_m^{\text{LD}} - \Delta\omega_y \right|^2}. \tag{54}$$

Note that the noise was assumed dipolar and white in Ref. [3], giving $|\hat{\xi}_0|^2 = \sigma_{\xi0}^2 f_{\text{rev}}$ for $\omega \in [0, \omega_0/2)$ and zero for other frequencies and noise signals. Here, $\sigma_{\xi0}$ is the rms amplitude of the noise kick per turn in units of the beam size. In addition, normalized units are used in Ref. [3], corresponding to $\beta_y = 1$. A factor β_y has therefore been added in the denominator of Eq. (54) to cancel that of the noise signal squared.

The derivation modeling the mode as an USHO made stronger assumptions on the dynamics and is therefore assumed to be less accurate than the new Vlasov-based theory. Even so, the only difference between the expressions is that the MTF in the Vlasov theory depends on the distance from the stability diagram to the undamped tune shift, $\Delta\Omega_m - \Delta\Omega_{l_m}^{\text{SD}}$, while the MTF in the USHO theory depends on the distance from the single-particle betatron frequency to the damped mode frequency, $\Delta\Omega_m^{\text{LD}} - \Delta\omega_y$. Separately, a great challenge with using the USHO theory, was the need to calculate $\Delta\Omega_m^{\text{LD}}$, which in Ref. [3] introduced additional assumptions and inaccuracies through the use of a Taylor expansion. Hence, the MTF and diffusion coefficient derived in this paper are both assumed closer to reality and do not require further assumptions to be calculated.

4.2 Comparison to multi-particle tracking simulations

The expressions derived for the diffusion coefficients will here be benchmarked against multi-particle tracking simulation run with COMBI. Since diffusion is a second-order effect, more simulations are needed to get an accurate estimate of the diffusion coefficient that depends on the spread of action $\langle \Delta J^2 \rangle$. 24 tracking simulations have been run with 10^7 macro-particles for each configuration. Only horizontal rigid white noise $\propto \Xi_0$ is modeled. The diffusion is presented in units of $D_0 = \sigma_{\xi0}^2/2\beta_x$, the diffusion expected due to noise in the absence of wakefields and a feedback system.

First, the diffusion due to a single mode with $\eta_{0m} = 1$ is studied. The wakefields are in COMBI modeled by an anti-damper, i.e., a kick that is constant over the bunch length and that is proportional to the average position offset. This simplified model allows for an easy control of the corresponding tune shift in the numerical simulations. The numerical diffusion coefficient is in Fig. 3 compared to the Vlasov theory in Eq. (52) and the USHO theory in Eq. (54). In Fig. 3a, the tested mode has a tune shift qualitatively similar to that of the most problematic modes in the LHC, with a significant negative real part relative to the imaginary part. The two theories are close to identical and agree well with the simulations. In Fig. 3b, the tested mode has a tune shift such that the Taylor
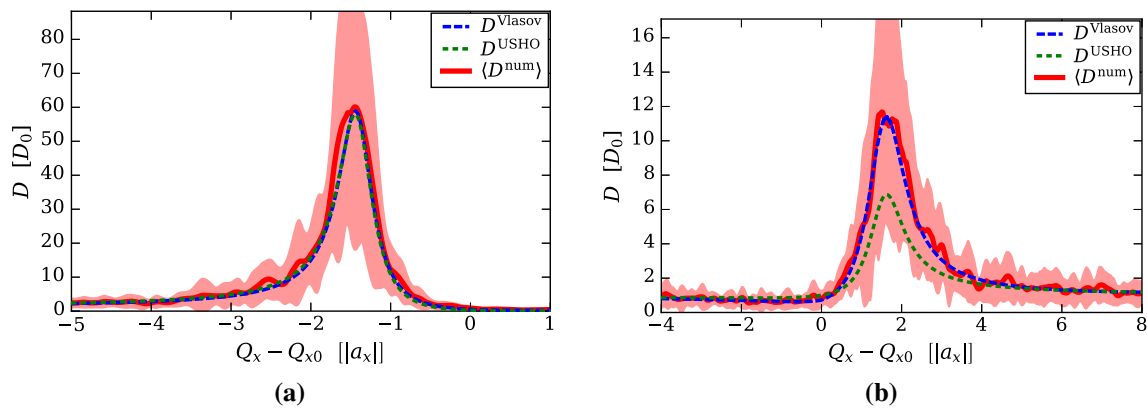
Fig. 3 Numerical diffusion calculated with COMBI compared to both the Vlasov and the USHO theories. The wakefields are driven by an anti-damper. In (**a**), the anti-damper represents a mode with complex tune shift $\Delta Q_x^{\mathrm{coh}} = -1.467 \times 10^{-3} + 1.25 \times 10^{-4}i$. In (**b**), the anti-damper drives a mode with $\Delta Q_x^{\mathrm{coh}} = 3.75 \times 10^{-4} + 5.504 \times 10^{-4}i$. Both of these modes have a stability threshold, in terms of detuning coefficients, of $a_x = 5 \times 10^{-4}$ and $b_x/a_x = -0.7$. Note that what matters is the phase of the complex tune, not the amplitude, together with the relative stability margin in octupole current, which is 50% in both configurations. The red shaded area corresponds to 1 standard deviation from the solid red line
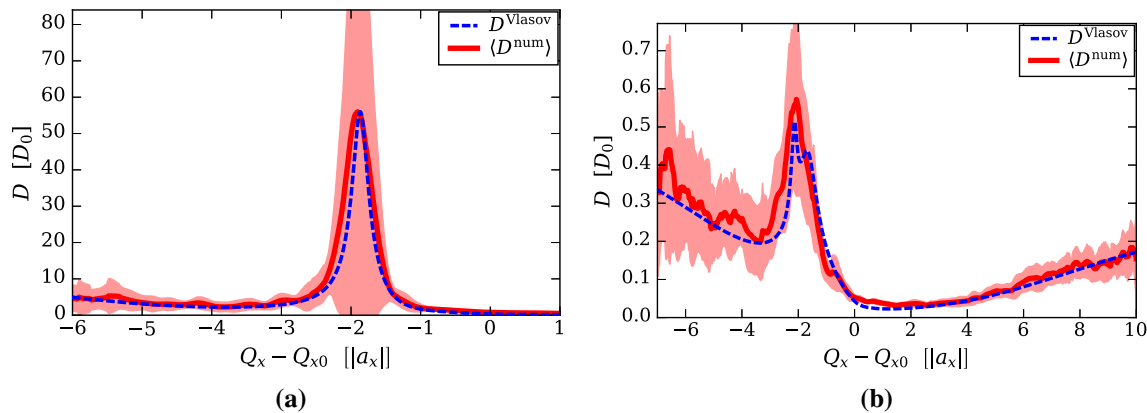
Fig. 4 Numerical diffusion calculated with COMBI compared to the Vlasov theory. The wakefields represent those in the LHC at top energy in 2018 with a linear chromaticity of $Q' = 15$. The feedback gain is 0 in (**a**) and corresponds to a damping time of 100 turns in (**b**). The stability margin in octupole current is 25% in both configurations. The red shaded area corresponds to 1 standard deviation from the solid red line

expansion used to get ΔQ_m^{LD} in the USHO theory is inaccurate. The Vlasov theory is found to be superior to the USHO theory for this mode. For this setup with one rigid mode, the Vlasov theory in Eq. (52) is identical to its inspiration in Ref. [19] when using a two-dimensional tune spread.

Second, the diffusion due to the full LHC wakefields will be studied. Calculations made with BimBim, using the impedance model for the LHC at top energy in 2018, have again been used to get the mode details. The bunch intensity, synchrotron tune, and rms particle momentum spread were the same as given in Table 1. The numerical diffusion coefficient is in Fig. 4 compared to the Vlasov theory in Eq. (51). There is good agreement both with and without a feedback. Note that the diffusion coefficient with a feedback is the sum of a multitude of D_m^{Vlasov}, driven by individual modes, which are shown individually in Fig. 5a. The sums for various stability margins are shown in Fig. 5b.

4.3 Distribution and stability evolution

The diffusion driven by noise and wakefields causes an evolution of the distribution, which leads to a change of the stability diagram since the latter is inversely proportional to the dispersion integral in Eq. (21). We consider here an illustrative example for the horizontal plane in the LHC at top energy in 2018 that is also considered in Ref. [22], with most parameters given in Table 1, a ratio between the detuning coefficients of $b_x/a_x = -0.7$, and a detuning coefficient a_x that is 25% larger than the initial stability threshold for a bunch with a Gaussian transverse distribution. This is the same case as is tested in Fig. 4b. The diffusion coefficient is a sum of a multitude of D_m^{Vlasov} that are shown individually in Fig. 5a. The modes that are inherently stable also without Landau damping, in part due to the feedback, are bowl-shaped, *i.e.*, zero at a center tune and increasing on both sides. This is qualitatively the same shape that is found in Ref. [23] for a bunch driven by noise and damped by a feedback system, in the absence of wakefields. It is found in Ref. [23] that diffusion coefficients of this shape are not critical for the loss of Landau damping that is observed in the
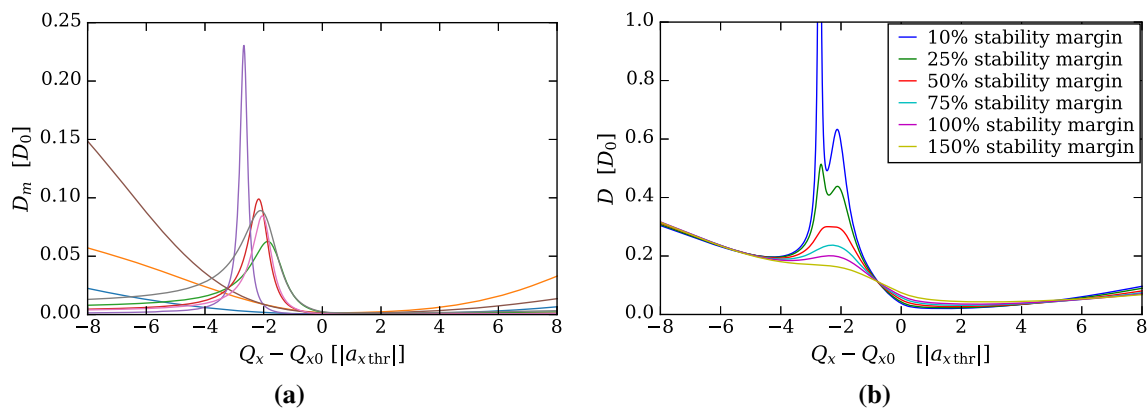
Fig. 5 Diffusion coefficient with the LHC wakefields, using the parameters in Table 1, according to the Vlasov theory in Eqs. (51) and (52). (**a**) displays the largest diffusion coefficients driven by individual wakefield-driven modes with a stability margin of 25%. The stability margin is a global measure, being the margin for the least stable mode, which corresponds to the most peaked line in (**a**). (**b**) displays the total diffusion coefficient for various stability margins. The green curve with 25% stability margin is equal to the blue curve in Fig. 4b and the sum of the curves in (**a**)

Table 1 Parameters for an LHC test case

Parameter	Value
Intensity, N	10^{11} p/b
Momentum spread, $\sigma_{\Delta p/p} = \sigma_z/\beta_z$	1.017×10^{-4}
Synchrotron tune, Q_s	0.00191
Linear chromaticity, Q'	15
Feedback damping time	100 turns
Rigid noise amplitude, $\sigma_{\xi 0}$	$10^{-4}\sigma_x$

Table 2 Latencies found with an anlytical equation and with several numerical simulations of different models [22]

Approach	Modes	Latency
Analytical equation[a]	The least stable one	144 s
USHO, simplified[b]	The least stable one	122 s
USHO	The least stable one	42 s
Vlasov	The least stable one	24 s
Vlasov	All	37 s

[a]Eq. (50) in Ref. [3], based on the USHO theory.
[b]Equal assumptions as when deriving Eq. (50) in Ref. [3]

LHC. On the other hand, the modes that would be unstable if not for Landau damping are peaked and narrow as the ones in Fig. 3. It is found in Ref. [3] that diffusion coefficients of this shape lead to a local flattening of the distribution in action space and a drilling of a hole in the stability diagram until the mode is unstable. This is the cause for loss of Landau damping after a latency that has been observed in the LHC.

The distribution and stability evolution according to the Vlasov theory, both driven by the diffusion of only the least stable mode and by the diffusion of all the modes, are presented in Fig. 6. These evolutions have been calculated using the code PYRADISE [3], using a 2000 × 2000 grid in transverse action space, equidistant in the transverse amplitudes $r \propto \sqrt{J}$. The latencies found in both simulations are gathered in Table 2, which also include the latencies found with the USHO theory numerically and analytically. The relative change of the distribution driven by only the least stable mode in Fig. 6a appears quite different from that driven by all the modes in Fig. 6c. However, what matters most is the local flattening of the distribution that is visible in both figures as a line across which particles have moved from the dark blue area on the left to the dark red area on the right. The stability diagram therefore evolves similarly due to only the least stable mode in Fig. 6b as due to all the modes in Fig. 6d. Since the additional modes drive a measurable diffusion that in this case partly counteracts the distribution evolution driven by the least stable mode, their inclusion increases the latency from 24 s to 37 s. This increase by about 50% is considered small on the vast scale of possible latencies [3], as will be exemplified in Sect. 4.4.
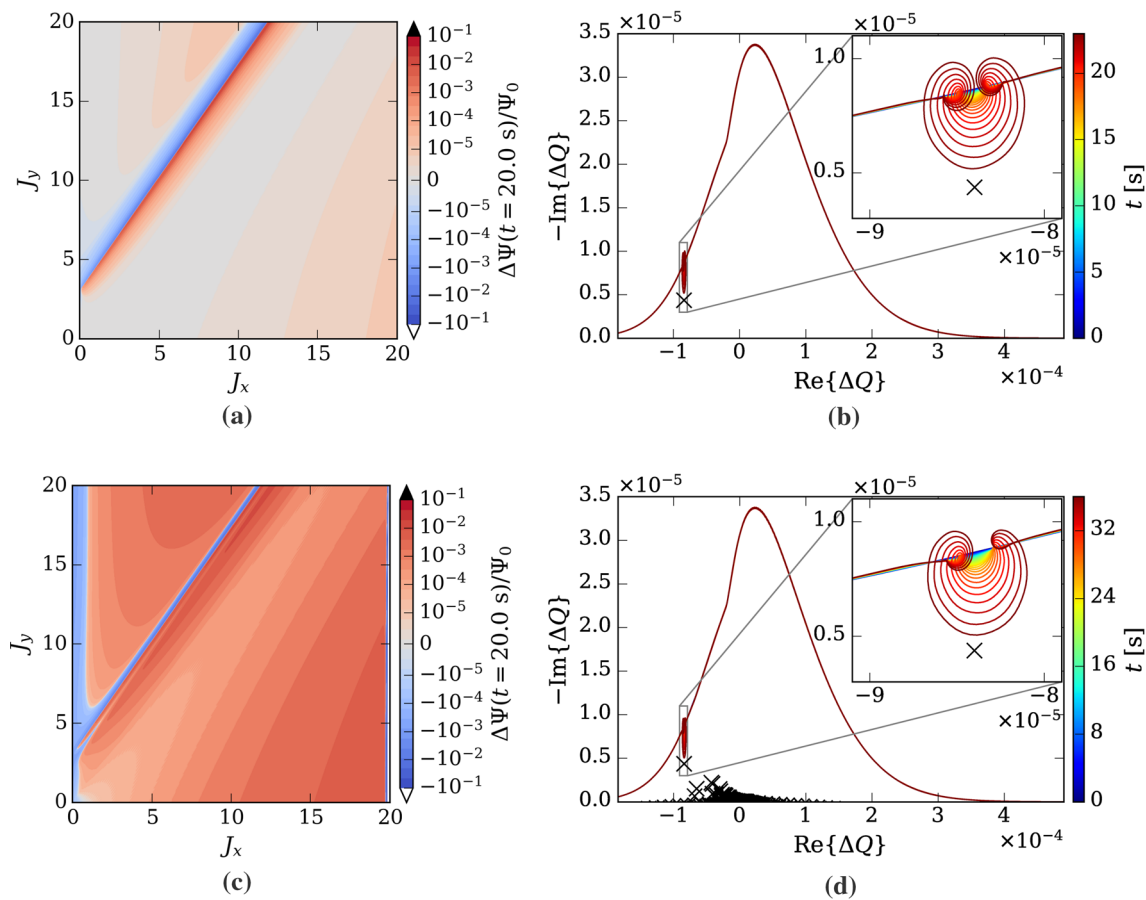
Fig. 6 `PyRADISE` simulations with the LHC wakefields, using the parameters in Table 1 and a stability margin of 25%. Relative change of the distribution on the left (a and c). Evolution of the stability diagram on the right (b and d), with the tune shifts ΔQ_m^{coh} of the modes marked by black crosses. Only the least stable mode is included on top (a and b), while all the modes are included on the bottom (c and d). The drilling of the hole in the stability diagram is only visualized until the initial stability margin is reduced by 75%, because of numerical effects discussed in Sect. 4.5

4.4 Dependence of latency on the stability margin

The latency depends on multiple key parameters, such as the noise and the noise-mode moments, but on none as critically as the stability margin, which is how much more detuning is used than necessary to stabilize a Gaussian beam. Here, this dependence will be illustrated by calculating the latency for the same test case as in Sect. 4.3, but with different stability margins.

The latencies calculated with the same five approaches as in Table 2 are shown in Fig. 7. There are many key results. First of all, the latency increases by more than 4 orders of magnitude by increasing the stability margin by 1 order of magnitude. Secondly, the analytical latency agrees well with the simplified simulation based on the USHO theory for all stability margins. This is expected, as the two approaches make the same assumptions. In general, the analytical latency gives an acceptable estimate also compared to the less simplified simulations, but it is slightly longer. The Vlasov and USHO theories with a single mode agree well, especially at small margins. Note that the Vlasov theory with a single mode has a numerical challenge at large stability margins that will be discussed in Sect. 4.5.

The model most true to the actual physics are the simulations based on the Vlasov theory including all the modes. This is also the most complex mechanism. The initial diffusion coefficient for different stability margins is displayed in Fig. 5b. At low margins, the peak due to the least stable mode is clearly visible, and it is this mode that eventually goes unstable. However, the diffusion due to the other modes slows down the destabilizing process. The latency with the Vlasov theory with all the modes is longer than the latency with only the least stable mode, and the difference increases with the stability margin, for small margins. Then, starting at a margin of 50% the peak due to the least stable mode is no longer visible in Fig. 5b and the total diffusion drills a wider hole. Eventually, it is actually a different mode that goes unstable, which is centered more in the middle of the peak of the total diffusion coefficient. This transition can also be seen in Fig. 7.

Fig. 7 Latency as a function of the stability margin for the LHC case otherwise described by the parameters in Table 1. The different curves correspond to different approaches (the same as in Table 2) to calculate the latency
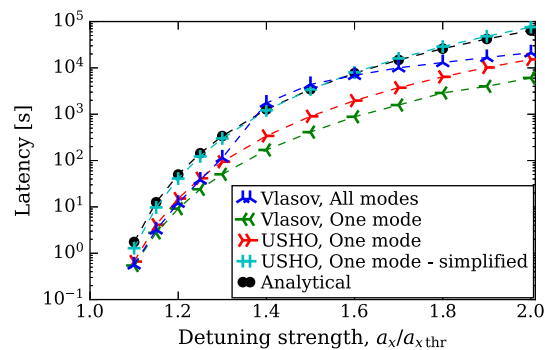
4.5 Discussion

Several aspects of this mechanism deserve further discussion. Here, we will discuss the physics, the differences between the USHO and the Vlasov theories, and various numerical challenges with both.

It is only the Vlasov theory that can accurately model the full wake-driven diffusion. The USHO theory can model the impact of additional almost unstable modes, but not the stable ones that cause the bowl-shaped diffusion coefficients exemplified in Fig. 5a. As also discussed in Ref. [3], it is challenging to predict the impact of the secondary modes in addition to the least stable one. In some cases, as the one tested here, they will extend the latency, but they may in principle also shorten it. If this level of understanding is required, it must be evaluated on a case-by-case basis.

The Vlasov theory for the MTF has been derived in this paper. It is illustrated in Fig. 3 that the Vlasov theory is more accurate than the more simplified USHO theory derived in Ref. [3]. However, the fact that the USHO theory allows for the derivation of an analytical equation for the latency (Eq. (50) in Ref. [3]) is quite useful. As shown in Fig. 7, the analytical estimate is in general within short range of the simulated latencies, in comparison with the many orders of magnitude over which the latency varies with the stability margin. Therefore, we suggest to use the analytical latency equation to estimate how much stability margin is required to achieve a desired latency. The required margin depends in particular on the noise and wakefield eigenmodes.

An aspect, which has not been focused on here, is the fact that the diffusion modeled by both theories is the expected motion as the number of turns goes to infinity. As seen by the variability between the separate simulations in Figs. 3 and 4, the expected diffusion coefficient is clearly not achieved each turn. This was discussed in more detail in Sect. IV.C in Ref. [3]. In fact, it was found that the wakefields driven by a mode particularly close to the stability limit drove a single-particle motion more comparable to resonant motion than diffusion.

A numerical issue has been discovered with the Vlasov theory. Loops start to develop at the edge of the drilled hole in the stability diagram when there is a large initial stability margin, especially when it models only a single mode. It is visible already in Fig. 6. These loops continue to grow so much that it interrupts the drilling of the initial hole, in addition to making the physical interpretation of the stability diagram challenging. We have found that this behavior is caused by initially insignificant details in the diffusion coefficient, which begin to enhance themselves. Based on the discussion in the previous paragraph, about the diffusion being the expected distribution evolution and not the actual evolution per turn, we believe this enhancement of minor details to be a non-physical consequence of the theory. Furthermore, this behavior is not reproduced with the USHO theory. For this reason, the latency is found by extrapolating the drilling from when the initial stability margin is reduced by 75%.

A final numerical challenge that we would like to point out is the convergence with numerical parameters. By reducing the discretization step in time and action space, the latency does converge towards a single value, as expected. Similarly, the stability diagram is calculated as the one-sided limit when the small parameter $\epsilon \to 0^+$ [6]. However, for $\epsilon \to 0^-$ and $\epsilon = 0$, one gets different results. In other words, the dispersion integral in Eq. (21) is discontinuous in the imaginary part of Ω, which causes numerical challenges for small positive values of ϵ. In the PyRADISE calculations presented here, we have used $\epsilon = |a_x|/200$, where a_x is the in-plane detuning coefficient due to octupole magnets. With this value of ϵ, the latency and stability diagram calculation appear to have converged, but it is quite close to a threshold below which the results are inaccurate due to the discontinuity of the dispersion integral.

5 Conclusion

In this paper, we have studied the excitation of beams in high-energy synchrotrons by noise. Within the framework of the linearized Vlasov equation, the MTF has been derived, modeling how a wakefield beam eigenmode is excited by noise. The initial excitation by noise depends on the shape of the eigenmode and the correlation of the noise along the bunch, modeled through the noise-mode moments η_{im}. The future evolution of the mode, after being excited by noise, depends on the strength of the wakefields and the

details of the detuning. It has here been assumed that the wakefields are weak, so that modes of different azimuthal mode numbers are linearly independent.

The BTF including chromaticity and wakefields has been derived based on the MTF. By comparing to multi-particle tracking simulations, it has been found that the new semi-analytical expression accurately models the impact of wakefields on the BTF. In particular, the shift of the BTF amplitude peaks in tune space has been thoroughly explained. The new theory can, in the limit of negligible wakefields, also be used to get an expression for the BTF including chromaticity. This expression also agrees excellently with multi-particle tracking simulations.

The main motivation for this work was to better understand the loss of Landau damping driven by noise and wakefields, which has been observed in the LHC. The MTF based on the linear Vlasov equation has been used to derive an expression for the diffusion driven by the interplay between noise and wakefields. The Vlasov-based theory can both model the diffusion driven by almost unstable modes, for which the diffusion coefficients are peaked in tune space, and the diffusion driven by inherently stable modes, for which the diffusion coefficients are bowl shaped in tune space. The peaked diffusion coefficients driven by the almost unstable modes can cause a local flattening of the distribution, leading to the drilling of a hole in the stability diagram. This mechanism can cause a loss of Landau damping. By comparing to multi-particle tracking simulations, the Vlasov theory is found superior to the previously derived USHO theory, which modeled the eigenmodes as underdamped stochastic harmonic oscillators. Nevertheless, by use of the PDE-solver PyRADISE, both theories produce similar latencies within about a factor 2, which is fairly close compared to the many orders of magnitude that the latency varies over. The main technique suggested to increase the latency and thereby mitigate the loss of Landau damping is to increase the stability margin, *i.e.*, operating with more detuning than predicted to barely stabilize a beam with a Gaussian transverse distribution. How much margin that is needed to achieve a certain latency depends in particular on the noise and wakefield eigenmodes and can be estimated with the analytical latency equation derived in Ref. [3].

Going forward, it will be of particular interest to study operational conditions of real accelerators with the new diffusion theory for the loss of Landau damping. For instance, the impact of crab cavity amplitude noise must be studied in detail to estimate the accepted noise levels in the HL-LHC. Such a study may also find alternative operational configurations, by *e.g.*, optimizing the linear chromaticity and gain of the transverse feedback system so that the latency is maximized.

Availability of data and material Not applicable.

Declarations

Conflict of interest Not applicable.

Code availability The codes used in this publication are available online (see references) or through direct contact.

Appendix A Calculating noise mode moments in DELPHI

We shall now explicit the expressions of the modes' sensitivity to different types of noise in the formalism implemented in the code DELPHI [14]. In the following, we consider only Gaussian longitudinal distributions.

The first noise type corresponds to a change of the transverse momentum of the particles that is independent of the particles' longitudinal coordinate at every turn, characterized by the function $\Xi_0 = 1$. This noise type is relevant for several applications, since the expected sources of noise can be current ripples in the power converters feeding the magnets, ground motion, or even active feedback systems. These phenomena are usually limited in bandwidth, such that the variations over the bunch length may be neglected. The second noise type corresponds to a change of the transverse momentum of the particles that is proportional to the particles' longitudinal coordinate. This noise type is relevant for the HL-LHC and future machines featuring crab cavities, as it is

expected due to voltage amplitude noise in these RF cavities. We characterize this noise with a function $\varXi_1 = z/\sigma_z$, where σ_z is the rms bunch length for a Gaussian distribution. These functions follow the normalization given by Eq. (36).

The code DELPHI seeks a distribution solution in the vertical plane of the type

$$m_m(r_z, \phi) = A_m e^{-i\frac{Q'_y r_z \cos(\phi)}{Q_s \beta_z}} \sum_{l=-\infty}^{\infty} R_l(r_z) e^{-il\phi}, \tag{A.1}$$

with

$$R_l(r_z) = \left(\frac{r_z}{4\sigma_z}\right)^{|l|} \sum_{n=0}^{\infty} c_l^n L_n^{|l|} \left(\frac{r_z^2}{2\sigma_z^2}\right), \tag{A.2}$$

where L_n are the generalized Laguerre polynomials of order n [5]. Note that in comparison with Eq. (33), here $g_0(r_z)$ is absorbed into R_l, and DELPHI do not need the assumption of weak wakefields, so that a mode here still contains the sum over all l. The factor A_m is determined such as to ensure the normalization given by Eq. (34). With a change of variable, we may identify the integral (4') in Ref. [24] and write

$$\langle m_m^* m_m \rangle_z = \frac{|A_m|^2}{2\pi\sigma_z^2} \sum_{l_1,l_2,n_1,n_2} c_{l_1}^{n_1*} c_{l_2}^{n_2} \iint dr_z d\phi r_z e^{-\frac{r_z^2}{2\sigma_z^2}} \left(\frac{r_z}{4\sigma_z}\right)^{|l_1|+|l_2|} L_{n_1}^{|l_1|}\left(\frac{r_z^2}{2\sigma_z^2}\right) L_{n_2}^{|l_2|}\left(\frac{r_z^2}{2\sigma_z^2}\right)$$

$$= |A_m|^2 \sum_{l_1,l_2,n_1,n_2} \frac{c_{l_1}^{n_1*} c_{l_2}^{n_2}}{8^{\frac{|l_1|+|l_2|}{2}}} \left[\frac{\Gamma(n_1+|l_1|+1)}{n_1!\Gamma(|l_1|+1)} \frac{\Gamma(n_2+|l_2|+1)}{n_2!\Gamma(|l_2|+1)} \Gamma\left(\frac{|l_1|+|l_2|}{2}+1\right) \right.$$

$$\left. \times F_2\left(\frac{|l_1|+|l_2|}{2}+1 : -n_1, -n_2; |l_1|+1, |l_2|+1; 1, 1\right) \right], \tag{A.3}$$

with Appell's hyper-geometric function $F_2(\cdot)$ [25]. With this normalization, we can now write the sensitivity to dipole noise ($\varXi_0$). First, we make use of the Jacobi–Anger expansion (Eq. (8.511.4) in Ref. [11]), such that the integration over the angle becomes trivial. Then, we may identify the integral (23) in Ref. [14] and write

$$\langle m_m^* \varXi_0 \rangle_z = \frac{A_m}{2\pi\sigma_z^2} \sum_{l,n} c_l^n \iint dr_z d\phi r_z e^{-\frac{r_z^2}{2\sigma_z^2}} e^{i\frac{Q'_y r_z \cos(\phi)}{Q_s \beta_z}} \left(\frac{r_z}{4\sigma_z}\right)^{|l|} L_n^{|l|}\left(\frac{r_z^2}{2\sigma_z^2}\right) e^{il\phi}$$

$$= A_m \sum_{l,n} c_l^n \frac{i^{-l}\mathrm{sign}(l)^{|l|}}{2^{2|l|+n}n!} \left(\frac{Q'_y \sigma_z}{Q_s \beta_z}\right)^{2n+|l|} e^{-\frac{Q'^2_y \sigma_z^2}{2Q_s^2 \beta_z^2}}. \tag{A.4}$$

We note that in the absence of chromaticity, only the mode with $n = l = 0$ is sensitive to dipole noise.

In order to obtain a closed form for the sensitivity to the second type of noise, we make again use of the Jacobi–Anger expansion together with Euler's formula for the cosine, so that we can write

$$\langle m_m^* \varXi_1 \rangle_z = \frac{A_m}{2\pi\sigma_z^3} \sum_{l,n} c_l^n \iint dr_z d\phi r_z^2 \cos(\phi) e^{-\frac{r_z^2}{2\sigma_z^2}} e^{i\frac{Q'_y r_z \cos(\phi)}{Q_s \beta_z}} \left(\frac{r_z}{4\sigma_z}\right)^{|l|} L_n^{|l|}\left(\frac{r_z^2}{2\sigma_z^2}\right) e^{il\phi}$$

$$= \frac{A_m}{2\sigma_z^3} \sum_{l,n} c_l^n \frac{i^{l+1}\mathrm{sign}(l)^{l+1}}{(4\sigma_z)^{|l|}} \int dr_z e^{-\frac{r_z^2}{2\sigma_z^2}} r_z^{|l|+2} L_n^{|l|}\left(\frac{r_z^2}{2\sigma_z^2}\right)$$

$$\times \left[J_{|l|+1}\left(\frac{Q'_y r_z}{Q_s \beta_z}\right) - J_{|l|-1}\left(\frac{Q'_y r_z}{Q_s \beta_z}\right) \right]. \tag{A.5}$$

In the last step, we introduced the absolute value of l in the index of the Bessel function using the identity (8.404.2) in Ref. [11]. If the chromaticity is 0, most of the terms in the sum are zero, the remaining ones are obtained using Eq. (7.414.7) in Ref. [11]

$$\langle m_m^* \varXi_1 \rangle_z = \frac{A_m}{4}(c_1^0 - c_{-1}^0). \tag{A.6}$$

Similarly to the dipole noise, only a few modes are sensitive to crab cavity amplitude noise in the absence of chromaticity, namely the ones with $n = 0$ and $l \pm 1$. In the general case, one may use the functional relations (8.971.4) and (8.971.5) in Ref. [11] to solve the integral involving the Bessel function with index $|l| - 1$ and $|l| + 1$, respectively. In both cases, the integral (23) in Ref. [14] can

be identified, so that we can write

$$\langle m_m^* \Xi_1 \rangle_z = A_m \sum_{l,n} c_l^n \frac{\text{sign}(l)^{l+1} i^{l+1}}{2^{2|l|+n} n!} \left(\frac{Q_y' \sigma_z}{Q_s \beta_z} \right)^{2n+|l|-1} \text{e}^{-\frac{1}{2} \left(\frac{Q_y' \sigma_z}{Q_s \beta_z} \right)^2} \left[\left(\frac{Q_y' \sigma_z}{Q_s \beta_z} \right)^2 - 2n - |l| \right]. \tag{A.7}$$

We note that the relation (8.971.5) is not valid for $n = 0$. Nevertheless, it can be shown that the expression obtained remains valid for $n = 0$ starting from Eq. (A.5), using the integral (6.631.1) in Ref. [11], identifying the relations with the confluent hyper-geometric function (9.215.1) and (9.212.1) in Ref. [11], exploiting the link between the confluent hyper-geometric function and Laguerre polynomials (8.972.1) in Ref. [11], and finally expressing the Laguerre polynomials with Eq. (8.973.2) in Ref. [11].

Appendix B Headtail beam transfer function with chromaticity

In this appendix, we will derive an alternative BTF to the one in Sect. 3.1. Here, both the external driving force and the measured response will have a linear headtail dependence, i.e., being proportional to $z = r_z \cos(\phi)$. The coherent force F_y^{coh} is now

$$F_y^{\text{coh}}(z, t) = r_z \cos(\phi) A_y \text{e}^{i\Omega t}, \tag{B.1}$$

which is qualitatively equivalent to crab cavity amplitude noise. The rms kick strength is $\text{rms}(F_y^{\text{coh}}) = \sigma_z A_y \text{e}^{i\Omega t}$, where σ_z is the rms longitudinal spread of the particles in the bunch. Putting it in Eq. (13) and using the Jacobi–Anger expansion (Eq. (8.511.4) in Ref. [11]) give

$$\sum_{l=-\infty}^{\infty} R_l(r_z) \text{e}^{-il\phi} (\Omega - \omega_0 Q_{y0} - l\omega_s) = \frac{A_y r_z}{4 p_0} g_0(r_z) \left(\text{e}^{i\phi} + \text{e}^{-i\phi} \right) \sum_{l=-\infty}^{\infty} i^l \text{e}^{il\phi} J_l \left(\frac{Q_y' r_z}{Q_s \beta_z} \right), \tag{B.2}$$

where $J_l(\cdot)$ are the Bessel functions of order l. By performing a term-by-term identification of terms with $\text{e}^{-il\phi}$, one gets an expression for the longitudinal modes

$$R_l(r_z) \text{e}^{-il\phi} = \frac{A_y r_z}{4 p_0} \frac{g_0(r_z)}{\Omega - \omega_0 Q_{y0} - l\omega_s}$$
$$\times \text{e}^{-il\phi} \left[i^{-l+1} J_{-l+1} \left(\frac{Q_y' r_z}{Q_s \beta_z} \right) + i^{-l-1} J_{-l-1} \left(\frac{Q_y' r_z}{Q_s \beta_z} \right) \right]. \tag{B.3}$$

Inserting this into the expression for the distribution perturbation in Eq. (12) gives

$$\Delta\Psi = \frac{A_y r_z}{4 p_0} \text{e}^{i\Omega t} \text{e}^{i\theta_y} \frac{\partial f_0}{\partial J_y} g_0(r_z) \sqrt{2 J_y \beta_y} \sum_{k,l} \frac{i^{l+1-k} \text{e}^{i(k-l)\phi}}{\Omega - \omega_0 Q_y(J_x, J_y) - l\omega_s} J_k \left(\frac{Q_y' r_z}{Q_s \beta_z} \right)$$
$$\times \left[J_{l+1} \left(\frac{Q_y' r_z}{Q_s \beta_z} \right) - J_{l-1} \left(\frac{Q_y' r_z}{Q_s \beta_z} \right) \right], \tag{B.4}$$

where we have again introduced the weak transverse detuning.

We are now in a position to calculate the headtail BTF (BTF$^{\text{ht}}$), the headtail beam response to a driving force that is proportional to z. The headtail beam moment is here defined normalized to the bunch length as

$$y^{\text{ht}} \equiv \left\langle \frac{yz}{\sigma_z} \right\rangle = \frac{\int_0^{2\pi} \text{d}\theta_x \int_0^{\infty} \text{d}J_x \int_0^{2\pi} \text{d}\theta_y \int_0^{\infty} \text{d}J_y \int_0^{2\pi} \text{d}\phi \int_0^{\infty} \text{d}J_z (\Psi_0 + \Delta\Psi) \sqrt{2 J_y \beta_y} \cos(\theta_y) r_z \cos(\phi)/\sigma_z}{\int_0^{2\pi} \text{d}\theta_x \int_0^{\infty} \text{d}J_x \int_0^{2\pi} \text{d}\theta_y \int_0^{\infty} \text{d}J_y \int_0^{2\pi} \text{d}\phi \int_0^{\infty} \text{d}J_z (\Psi_0 + \Delta\Psi)}. \tag{B.5}$$

By insertion, one finds

$$\text{BTF}^{\text{ht}} \equiv \frac{y^{\text{ht}}}{\text{rms}(F_y^{\text{coh}})} \frac{p_0}{\beta_y} = \sum_l \mathcal{T}_l(\Omega) w_{1l}(Q_y'), \tag{B.6}$$

which again depends on the dispersion integral in Eq. (21) and a weight that depends on chromaticity

$$w_{1l}(Q_y') \equiv \frac{\pi}{2} \int_0^{\infty} \left[J_{l+1} \left(\frac{Q_y' r_z}{Q_s \beta_z} \right) - J_{l-1} \left(\frac{Q_y' r_z}{Q_s \beta_z} \right) \right]^2 \frac{r_z^2}{\sigma_z^2} g_0(r_z) \frac{r_z \text{d}r_z}{\beta_z}. \tag{B.7}$$

In the absence of chromaticity, w_{1l} is 0.5 for $l = \pm 1$ and 0 otherwise.

We can also express the BTF$^\text{ht}$ based on the MTF derived in Sect. 3.2. The headtail mode moment can be found as

$$y_m^\text{ht}(t) = \left\langle \frac{yz}{\sigma_z} \right\rangle = \chi_m \langle \Xi_1^* m_m \rangle_z = \chi_m \tilde{\eta}_{1\,m}^*, \tag{B.8}$$

where it was used that $\Xi_1 = z/\sigma_z$. By combining this with Eq. (40) and assuming only noise proportional to Ξ_1, we get the desired expression for the headtail BTF$^\text{ht}$ including wakefields

$$\text{BTF}^\text{ht} = \frac{\hat{y}^\text{ht}(\Omega)}{\hat{\xi}_1(\Omega)} = \frac{\sum_m \hat{y}_m^\text{ht}(\Omega)}{\hat{\xi}_1(\Omega)} = \sum_m \mathcal{T}_{l_m}^\text{wake}(\Omega) \tilde{\eta}_{1\,m}^* \eta_{1\,m}, \tag{B.9}$$

where $\mathcal{T}_{l_m}^\text{wake}(\Omega)$ is defined in Eq. (40). In the limit of negligible wakefields but still including chromaticity, such that $\mathcal{T}_{l_m}^\text{wake} \to \mathcal{T}_l$, we can calculate the weight of sideband l as

$$w_{1l}^\text{MTF} = \sum_m \tilde{\eta}_{1\,m}^* \eta_{1\,m} \delta_{l,l_m}, \tag{B.10}$$

which is readily comparable to the weight w_{1l} in Eq. (B.7).

References

1. S.V. Furuseth, X. Buffat, Instability Latency in the LHC. In: M. Boland, H. Tanaka, and D. Button (eds) Proceedings of the 10th Int. Particle Accelerator Conf. (IPAC19), JACoW, Melbourne, Australia, May 2019, pp. 3204–3207 (2019), https://doi.org/10.18429/JACoW-IPAC2019-WEPTS044
2. S. V. Furuseth, X. Buffat, E. Métral, D. Valuch, B. Salvant, D. Amorim, N. Mounet, M. Söderén, S. A. Antipov, T. Pieloni, C. Tambasco, MD3288: Instability latency with controlled noise. CERN, Geneva, Switzerland, Rep. CERN-ACC-NOTE-2019-0011 (2019)
3. S.V. Furuseth, X. Buffat, Phys. Rev. Accel. Beams **23**, 114401 (2020). https://doi.org/10.1103/PhysRevAccelBeams.23.114401
4. S.V. Furuseth, Transverse Noise, Decoherence, and Landau Damping in High-Energy Hadron Colliders. Ph.D. dissertation, École polytechnique fédérale de Lausanne, Lausanne, Switzerland, (2021) https://doi.org/10.5075/epfl-thesis-9330
5. N. Mounet, Direct Vlasov Solvers. In: Proceedings of the 2018 course on numerical methods for analysis, design and modelling of particle accelerators, Thessaloniki, Greece, CERN, 11–23 Nov 2018, p. 300 (2020)
6. J.S. Berg, F. Ruggiero, Landau damping with two-dimensional betatron tune spread. CERN, Geneva, Switzerland, Rep. CERN-SL-96-071-AP (1996)
7. C. Tambasco, T. Pieloni, X. Buffat, E. Métral, Beam transfer function and stability diagram in the Large Hadron Collider. In: E. Métral, G. Rumolo, T. Pieloni (eds) Proceedings of the ICFA mini-Workshop on Mitigation of Coherent Beam Instabilities in Particle Accelerators, Zermatt, Switzerland, Sep 2019, pp. 115–120 (2020), https://doi.org/10.23732/CYRCP-2020-009.115
8. T. Nakamura, Excitation of betatron oscillation under finite chromaticity. Paper presented at the 12th Symposium on Accelerator Science and Technology, Wako, Japan, 27–29 Oct 1999, p. 534-536 (1999), http://www.spring8.or.jp/pdf/en/ann_rep/98/P121-123.pdf
9. A. Chao, *Physics of Collective Beams Instabilities in High Energy Accelerators* (Wiley, New York, 1993)
10. H. Goldstein, J. Safko, C. Poole, Classical Mechanics 3rd edn. (London, Pearson Education, 2014)
11. I.S. Gradshteyn, I.M. Ryzhik, *Table of Integrals, Series, and Products*, 6th edn. (San Diego, Academic Press, 2000)
12. J. Gareyte, J.P. Koutchouk, F. Ruggiero, Landau damping, dynamic aperture and octupoles in LHC. CERN, Geneva, Switzerland, Rep. CERN-LHC-PROJECT-REPORT-091 (1997)
13. F.J. Sacherer, Methods for computing bunched-beam instabilities. CERN, Geneva, Switzerland, Rep. CERN-SI-BR-72-5 (1972)
14. N. Mounet, Vlasov solvers and macroparticle simulations. In: proceedings of the ICFA mini-workshop on impedances and beam instabilities in particle accelerators, Benevento, Italy, 18–22 Sep 2017, (2018) https://doi.org/10.23732/CYRCP-2018-001.77
15. X. Buffat, Transverse beams stability studies at the Large Hadron Collider. Ph.D. dissertation, École polytechnique fédérale de Lausanne, Lausanne, Switzerland (2015), https://doi.org/10.5075/epfl-thesis-6321
16. S.V. Furuseth, X. Buffat, Comput. Phys. Commun. **244**, 180–186 (2019). https://doi.org/10.1016/j.cpc.2019.06.006
17. S.V. Furuseth, X. Buffat, T. Pieloni, W. Herr, F. Jones, COMBI (COherent Multi-Bunch Interactions) (2021). https://cern.ch/combi/. Accessed 1 Apr 2021
18. X. Buffat, Theory of transverse beam transfer function with chromaticity (2020). https://indico.cern.ch/event/980131/contributions/4130522/. Accessed 29 Apr 2021
19. V. Lebedev, Damping rate limitations for transverse dampers in large hadron colliders. In: E. Métral, G. Rumolo, T. Pieloni (eds) Proceedings of the ICFA mini-Workshop on Mitigation of Coherent Beam Instabilities in Particle Accelerators, Zermatt, Switzerland, Sep 2019, pp. 203–210 (2020), https://doi.org/10.23732/CYRCP-2020-009.203
20. A. Bazzani, S. Siboni, G. Turchetti, Physica D **76**, 8–21 (1994). https://doi.org/10.1016/0167-2789(94)90246-1
21. A. Bazzani, L. Beccaceci, J. Phys. A: Math. Gen. **31**, 5843–5854 (1998). https://doi.org/10.1088/0305-4470/31/28/004
22. S.V. Furuseth, X. Buffat, Loss of Transverse Landau Damping by Diffusion in High-Energy Hadron Colliders. In: Proceedings of the 12th Int. Particle Accelerator Conf. (IPAC21), JACoW, Campinas, SP, Brasil, 24–28 May 2021, paper TUXA06 (in press) (2021)
23. S.V. Furuseth, X. Buffat, Phys. Rev. Accel. Beams **23**, 034401 (2020). https://doi.org/10.1103/PhysRevAccelBeams.23.034401
24. A. Erdélyi, Math Z **40**, 693–702 (1936). https://doi.org/10.1007/BF01218891
25. P. Appell, Journal de Mathématiques Pures et Appliquées. (3ème série) **8**, pp. 173–216 (1882)